Eur. Phys. J. C 23, 513–526 (2002)
Digital Object Identifier (DOI) 10.1007/s100520200893

THE EUROPEAN PHYSICAL JOURNAL C

Saturation model for two-photon interactions at high energies

N. Tîmneanu[1], J. Kwieciński[2], L. Motyka[1,3]

[1] High Energy Physics, Uppsala University, 75 121 Uppsala, Sweden
[2] H. Niewodniczański Institute of Nuclear Physics, 31-342 Kraków, Poland
[3] Institute of Physics, Jagellonian University, 30-059 Kraków, Poland

Received: 1 November 2001 /
Published online: 15 March 2002 –

Abstract. We formulate and analyse a saturation model for the total $\gamma\gamma$ and $\gamma^*\gamma^*$ cross-sections and for the real photon structure function $F_2^\gamma(x,Q^2)$. The model is based on a picture in which the $\gamma^*\gamma^*$ total cross-section for arbitrary photon virtualities is driven by the interaction of colour dipoles into which the virtual photons fluctuate. The cross-section describing this interaction is assumed to satisfy the saturation property with the saturation radius taken from the Golec-Biernat and Wüsthoff analysis of the γ^*p interaction at HERA. The model is supplemented by the QPM and non-pomeron reggeon contributions. The model gives a very good description of the data on the $\gamma\gamma$ total cross-section, on the photon structure function $F_2^\gamma(x,Q^2)$ at low x and on the $\gamma^*\gamma^*$ cross-section extracted from LEP double tagged events. The production of heavy flavours in $\gamma\gamma$ collisions is also studied. Predictions of the model for the very high energy range which will be probed at future linear colliders are given.

1 Introduction

The concept of parton density saturation in high energy scattering mediated by strong interactions is certainly one of the most interesting recent developments in QCD theory and phenomenology [1–16]. It is well known that the cross-sections for processes characterised by a large scale Q^2 exhibit a steep power-like increase with the collision center of mass energy squared W^2, when $W^2 \gg Q^2$. Such an increase, attributed to the so-called hard pomeron [1, 17], if continued to arbitrarily large energies, would eventually lead to break-down of the S-matrix unitarity. To avoid the apparent unitarity violation, effects related to screening (shadowing) phenomena have to be considered. They correspond to multiple bare pomeron exchanges and multi-pomeron interactions, and tame the steep increase at high energies. In the language of parton densities, the cross-section increases as the number of partons grows in the target, due to gluon emissions into the available rapidity interval, $Y \sim \ln(W^2/Q^2)$. This growth may be described as evolution in rapidity, with the evolution length Y. However, apart from creation of new partons the competing phenomenon of gluon recombination occurs, which reduces the number of partons. The recombination becomes increasingly important at high parton densities, i.e. for a large evolution length Y. This qualitative picture has a solid theoretical basis, well rooted in QCD [1–15].

A very non-trivial feature which arises from those studies is that the characteristic rapidity evolution length Y, for which the unitarity corrections become important, depends on the hard scale Q^2. This statement may be inverted, leading to the notion of the Y-dependent saturation scale $Q_\mathrm{s}(Y)$, the characteristic scale for the transition between colour transparency and saturated cross-section regimes, at given rapidity Y. This phenomenon has recently been thoroughly studied through the measurement of ep inelastic scattering at HERA within a broad range of Q^2 varying from the DIS large Q^2 region down to the real photoproduction limit $Q^2 \approx 0$ [18]. Here $Q^2 = -q^2$, where q is the four-momentum transfer in the process $ep \to e'X$. Since this process is largely controlled by one photon exchange, Q^2 corresponds to the photon virtuality. Measurement of ep inelastic scattering permits determination of the virtual photon–proton total cross-section $\sigma_{\gamma^*p}(Q^2,W^2)$ for all virtual photon polarisation states, with W being the photon–proton collision energy.

Golec-Biernat and Wüsthoff (GBW) managed to fit these data in a model incorporating the saturation property, with rapidity dependent saturation scale [16]. In this case the γ^*p cross-section is described in terms of the $q\bar{q}$ colour dipoles which the (virtual) photon fluctuates to according to a known wave function. The dipoles scatter off the proton with a cross-section which exhibits the colour transparency and the saturation property in the limit of a small dipole size, $r \ll 1/Q_\mathrm{s}(Y)$, and a large dipole size, $r \gg 1/Q_\mathrm{s}(Y)$, respectively. It is an encouraging result that the predictions of the simple model agree well with all the large rapidity data ranging from photoproduction to large Q^2. This model would therefore provide a description of the transition between the soft and hard high energy scattering in QCD. The same model explains also properties of the cross-section for hard diffraction at HERA, in partic-

ular the ratio of the total to diffractive cross-section being constant with energy [19].

Thus, it is important to perform other tests of the GBW model which probe its universality. Two virtual photon interactions at high energies offer an ideal opportunity for such studies since virtualities of both photons can vary, so that the properties of the model may be studied more extensively. Besides that, in the GBW model, the photon wave function is known, contrary to the proton wave function, so the two-photon data may be used to constrain the dipole–dipole cross-section itself.

There exist several models of two-photon interactions which aim at describing the variation of the dynamics depending on the photon virtualities [20–28]. Most of those models combine the vector meson dominance with the parton model suitably extended to the region of low virtualities. They do also usually rely on the Regge pole description of the high energy behaviour of the total cross-sections. Some of the models describing the total cross-sections of real photons explore the minijet production mechanism [29,30]. The $\gamma^*\gamma^*$ interactions have also been described within the dipole picture [23–25], but possible saturation properties of the dipole–dipole cross-section have not been studied so far. The saturation ansatz may be useful to better understand the features of the available two-photon data and to formulate some interesting predictions for the two-photon physics at future linear colliders.

In this paper we construct a generalisation of the saturation model for the two-photon case, compare its predictions with the experimental data and discuss the implications. The contents of our paper are as follows. In the next section we recall the GBW saturation model for γ^*p scattering and present its formulation for $\gamma^*\gamma^*$ high energy interactions. We point out that by a suitable choice of the quark masses, the model can be used to describe the total $\gamma\gamma$ cross-section for two real photons, the $\gamma^*\gamma^*$ total cross-section for two virtual photons measured in double tagged $e^+e^- \to e^+e^- + X$ events and the photon structure function $F_2^\gamma(x, Q^2)$ of real (or virtual) photon for low values of the Bjorken parameter x. We show that in the region where the saturation effects become important the model gives a steeper dependence of the cross-section on the collision energy than that obtained in the case of γ^*p scattering. In Sect. 3 we present a comparison with the available experimental data on $\sigma_{\gamma\gamma}$, $\sigma_{\gamma^*\gamma^*}$, $F_2^\gamma(x, Q^2)$ at low x and for the cross-section describing heavy flavour production in $\gamma\gamma$ collisions. Section 4 contains our predictions for the above quantities in the very high energy regime, which may be available in future linear ee, γe or $\gamma\gamma$ colliders. Finally in Sect. 5 we present a summary of our results.

2 The saturation model

2.1 The Golec-Biernat–Wüsthoff model

The study of the total virtual photon–proton cross-section in the high W limit and for Q^2 ranging from small to large values allows probing the transition from large to short distance physics in high energy scattering. Numerous analyses exist which study this transition [18,31]. Among them, a very successful description is provided by the saturation model developed by Golec-Biernat and Wüsthoff [16], in which the γ^*p scattering is viewed as the scattering between $(q\bar{q})_{\rm dipole}$ and the proton. The colour dipoles $(q\bar{q})_{\rm dipole}$ represent virtual components of the photon in the transverse plane (the plane transverse to the collision axis) and their distribution in the photon can be obtained in the perturbative framework.

The cross-section $\sigma_i^{\gamma^* p}(Q^2, W^2)$ for the transversely ($i = \mathrm{T}$) and longitudinally ($i = \mathrm{L}$) polarised virtual photon is given by the following formula:

$$\sigma_i^{\gamma^* p}(Q^2, W^2) = \int_0^1 \mathrm{d}z \int \mathrm{d}^2\boldsymbol{r}\, |\Psi_i(z, \boldsymbol{r})|^2 \hat{\sigma}(x, r^2), \quad (1)$$

where $\boldsymbol{r}$ denotes the transverse separation between q and $\bar{q}$ in the colour dipole, z is the longitudinal momentum fraction of the quark in the photon and x is the Bjorken parameter, i.e. $x = Q^2/(2pq)$. The cross-section $\hat{\sigma}(x, r^2)$ is the $(q\bar{q})_{\rm dipole}$–proton total cross-section, and $|\Psi_i(z, \mathbf{r})|^2$ denotes the photon wave function squared and summed over the quark helicities, in the photon polarisation state indicated by i. The photon wave function is given by its quark flavour decomposition

$$|\Psi_i(z, \boldsymbol{r})|^2 = \sum_f |\Psi_i^f(z, \boldsymbol{r})|^2, \quad (2)$$

and

$$|\Psi_i^f(z, \boldsymbol{r})|^2 = \frac{6\alpha_{\rm em}}{4\pi^2} e_f^2 \times \begin{cases} [z^2 + (1-z)^2]\epsilon_f^2 K_1^2(\epsilon_f r) + m_f^2 K_0^2(\epsilon_f r), \\ \qquad\qquad \text{for } i = \mathrm{T}, \\ 4Q^2 z^2 (1-z)^2 K_0^2(\epsilon_f r), \text{ for } i = \mathrm{L}, \end{cases} \quad (3)$$

with

$$\epsilon_f^2 = z(1-z)Q^2 + m_f^2, \quad (4)$$

where e_f and m_f denote the charge and mass of the quark of flavour f. The functions K_0 and K_1 are the McDonald–Bessel functions.

Equation (1) is in fact equivalent to the k_t (or high energy) factorisation, which is the basic tool for calculating the observable quantities at low x [32], and the dipole–proton cross-section $\hat{\sigma}(x, r^2)$ is related to the unintegrated gluon distribution in the proton $f(x, k^2)$ [33]

$$\hat{\sigma}(x, r^2) = \frac{4\pi\alpha_{\rm s}}{N_c} \int \frac{\mathrm{d}^2\boldsymbol{k}}{k^4} [1 - J_0(kr)] f(x, k^2). \quad (5)$$

In (5), $\boldsymbol{k}$ is the transverse momentum of the gluon and $J_0(z)$ is the Bessel function. In the leading $\ln(1/x)$ approximation, the unintegrated gluon distribution $f(x, k^2)$ is given by the solution of the BFKL equation which determines the "hard" pomeron in the perturbative QCD [17]. The exchange of the perturbative QCD pomeron however violates unitarity at very large energies. The novel feature

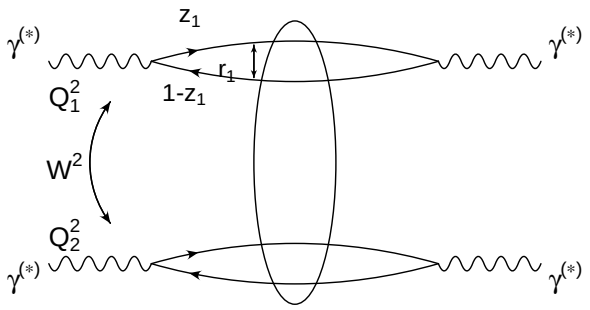

Fig. 1. The diagram illustrating the $\gamma^*\gamma^*$ interaction in the dipole representation; see (8)

of the saturation model is the incorporation of the unitarity constraint on the level of the dipole–proton cross-section $\hat{\sigma}(x, r^2)$. This is achieved by imposing the saturation property, i.e. $\hat{\sigma}(x, r^2) \to \sigma_0$ for $r \gg R_0(x)$, where the saturation radius $R_0(x)$ is a decreasing function with decreasing x:

$$R_0^2(x) \sim x^\lambda, \tag{6}$$

and the cross-section σ_0 is independent of x. In the limit $r \to 0$, it follows from the perturbative QCD calculations that the dipole cross-section exhibits the colour transparency property behaving as $\hat{\sigma}(x, r^2) \sim r^2/R_0^2(x)$ (modulo a logarithmic correction which can modify the r dependence). Those two properties are economically summarised by the following simple parametrisation:

$$\hat{\sigma}(x, r^2) = \sigma_0[1 - \exp(-r^2/(4R_0^2(x)))]. \tag{7}$$

2.2 Generalisation of the GBW model for the two-photon cross-section

The description of the $\gamma^*\gamma^*$ total cross-sections within the formalism utilising the interaction of two colour dipoles, which the virtual photons fluctuate into, has been discussed in detail in [23–25]. The dipole–dipole cross-sections were assumed to be given by the stochastic vacuum model [23,24] or to follow from the BFKL formalism [25]. The novel feature of our approach is the incorporation of the saturation property of the dipole–dipole cross-section. This makes it possible, in particular, to describe in a unified way the variation of the energy dependence of the cross-sections with the change of the virtualities of the photons. In terms of the virtual photon four-momenta q_1 and q_2 we have $Q_{1,2}^2 = -q_{1,2}^2$ and $W^2 = (q_1 + q_2)^2$; see Fig. 1. The extension of the saturation model to the case of $\gamma^*(Q_1^2)\gamma^*(Q_2^2)$ cross-sections for arbitrary virtualities $Q_{1,2}^2$ is given below.

A formula for the two-photon cross-section part coming from the exchange of *gluonic* degrees of freedom reads [23,24]

$$\sigma_{ij}^G(W^2, Q_1^2, Q_2^2) = \sum_{a,b=1}^{N_f} \int_0^1 \mathrm{d}z_1 \int \mathrm{d}^2\boldsymbol{r}_1 |\Psi_i^a(z_1, \boldsymbol{r}_1)|^2 \times \int_0^1 \mathrm{d}z_2 \int \mathrm{d}^2\boldsymbol{r}_2 |\Psi_j^b(z_2, \boldsymbol{r}_2)|^2 \sigma_{a,b}^{dd}(\bar{x}_{ab}, r_1, r_2), \tag{8}$$

where the indices i, j label the polarisation states of the virtual photons, i.e. T or L. The wave functions $\Psi_i^a(z_k, \mathbf{r})$ are given by (3), with ϵ_f^2 defined by (4) being replaced by $(\epsilon_f^k)^2 = z_k(1 - z_k)Q_k^2 + m_f^2$, $k = 1, 2$ and $\sigma_{a,b}^{dd}(\bar{x}_{ab}, r_1, r_2)$ are the dipole–dipole total cross-sections corresponding to their different flavour content specified by the a and b.

Inspired by the simple GBW choice for the dipole–proton cross-section, we use the following parametrisation of the dipole–dipole cross-section $\sigma_{a,b}(\bar{x}_{ab}, r_1, r_2)$:

$$\sigma_{a,b}^{dd}(\bar{x}_{ab}, r_1, r_2) = \sigma_0^{a,b}\left[1 - \exp\left(-\frac{r_{\mathrm{eff}}^2}{4R_0^2(\bar{x}_{ab})}\right)\right], \tag{9}$$

where for $\bar{x}_{ab}$ we take the following expression symmetric in $(1, 2)$

$$\bar{x}_{ab} = \frac{Q_1^2 + Q_2^2 + 4m_a^2 + 4m_b^2}{W^2 + Q_1^2 + Q_2^2}, \tag{10}$$

which allows an extension of the model down to the limit $Q_{1,2}^2 = 0$. Note that $\bar{x}_{ab}$ depends on the flavour of scattering quarks. We use the same parametrisation of the saturation radius $R_0(\bar{x})$ as that in (7) in [16], i.e.

$$R_0(\bar{x}) = \frac{1}{Q_0}\left(\frac{\bar{x}}{x_0}\right)^{\lambda/2}, \tag{11}$$

and adopt the same set of parameters defining this quantity as those in [16]. For the saturation value $\sigma_0^{a,b}$ of the dipole–dipole cross-section (cf. (9)) we set

$$\sigma_0^{a,b} = \frac{2}{3}\sigma_0, \tag{12}$$

where σ_0 is the same as that in [16]. For light flavours, (12) can be justified by the quark counting rule, as the ratio between the number of constituent quarks in a photon and the corresponding number of constituent quarks in the proton. Following [16], we use the same value of $\sigma_0^{a,b}$ for all flavours.

Three scenarios for $r_{\mathrm{eff}}(r_1, r_2)$ are considered:

(1) $r_{\mathrm{eff}}^2 = \dfrac{r_1^2 r_2^2}{r_1^2 + r_2^2}$;
(2) $r_{\mathrm{eff}}^2 = \min(r_1^2, r_2^2)$;
(3) $r_{\mathrm{eff}}^2 = \min(r_1^2, r_2^2)[1 + \ln(\max(r_1, r_2)/\min(r_1, r_2))]$.

The first two cases are simple generalisations of the parametrisation adopted in the case of the dipole–hadron scattering, i.e. we get $r_{\mathrm{eff}}^2 \sim r_1^2$ ($r_{\mathrm{eff}}^2 \sim r_2^2$) in the configurations $r_2^2 \gg r_1^2$ ($r_1^2 \gg r_2^2$). Case (3) is motivated by the two-gluon exchange between the colour dipoles, giving the following cross-section:

$$\sigma_{dd}^{2g} \sim 2\int \frac{\mathrm{d}k^2}{k^4}[1 - J_0(kr_1)][1 - J_0(kr_2)] = \min(r_1^2, r_2^2)[1 + \ln(\max(r_1, r_2)/\min(r_1, r_2))]. \tag{13}$$

In all three cases the dipole–dipole cross-section exhibits colour transparency, i.e. $\sigma_{a,b}^{dd}(\bar{x}, r_1, r_2) \to 0$ for $r_1 \to 0$ or $r_2 \to 0$.

The formulae given above correspond to the "pomeron" contribution to the $\gamma^*\gamma^*$ total cross-sections. This means that they represent the exchange of gluonic degrees of freedom giving rise to the component of cross-sections which, at high energies, does not decrease with increasing energy. Equation (9), defining the dipole–dipole cross-section, similarly to (7) for the dipole–proton cross-section, interpolates between the "hard pomeron" at small transverse separations $r_{1,2}$ and the "soft pomeron" at large transverse separations. In more detail, for small values of r_i (i.e. for $r_{\rm eff}^2 \ll 4R_0^2(\bar{x})$) one gets

$$\sigma_{a,b}^{dd}(\bar{x}_{ab}, r_1, r_2) \simeq \sigma_0^{a,b} \frac{r_{\rm eff}^2}{4R_0^2(\bar{x}_{ab})} \sim \bar{x}_{ab}^{-\lambda}, \qquad (14)$$

which can be interpreted as the "hard pomeron" contribution if the parameter λ is identified with the "hard pomeron" intercept. On the other hand for large dipole sizes we have

$$\sigma_{a,b}^{dd}(\bar{x}_{ab}, r_1, r_2) \sim \sigma_0^{a,b}, \qquad (15)$$

i.e. the cross-section is only slowly varying with the energy in accordance with what is observed for the "soft pomeron". It should be emphasised that the structure of the saturation model is different from that corresponding to two separate (i.e. "hard" and "soft") pomeron contributions [34]. The soft pomeron in the saturation model appears rather as an effect of unitarisation of the exchange amplitude of the "hard" contribution, provided by multiple exchanges and self-interaction of the "hard" pomerons.

2.3 Scaling of the cross-sections

The virtualities of the two photons can be arbitrary; thus the model can describe the following three cases of physical and phenomenological interest:

(1) The case $Q_1^2 = Q_2^2 = 0$ corresponding to the interaction of two real photons.
(2) The case $Q_1^2 \sim Q_2^2$ (with large $Q_{1,2}^2$) corresponding to the interaction of two (highly) virtual photons. The relevant cross-section can be extracted from the measurement of double tagged events $e^+e^- \to e^+e^- +$ *hadrons*.
(3) The case $Q_1^2 \gg Q_2^2$ corresponding to probing the structure of virtual ($Q_2^2 > 0$) or real ($Q_2^2 = 0$) photon at small values of the Bjorken parameter $x = Q_1^2/(2q_1q_2)$. For instance, the structure function $F_2^\gamma(x, Q^2)$ of the real photon ($Q_2^2 = 0, Q_1^2 = Q^2$) is related in the following way to the $\gamma^*\gamma$ total cross-sections:

$$F_2^\gamma(x, Q^2) = \frac{Q^2}{4\pi^2\alpha_{\rm em}} \times [\sigma_{\rm T,T}(W^2, Q^2, Q_2^2 = 0) + \sigma_{\rm L,T}(W^2, Q^2, Q_2^2 = 0)]. \qquad (16)$$

Let us now examine the high energy limit in all three cases and compare them with the γ^*p case. We shall show that in the kinematical configurations in which the saturation effects are important, the two-photon cross-sections are more singular in the high energy limit than the γ^*p cross-section. To be precise, the high energy behaviour of the total $\gamma^*\gamma^*$ cross-sections will be enhanced by additional factors of the large logarithm $\ln[Q^2R_0^2(\bar{x})]$. Also the behaviour of the $\gamma\gamma$ total cross-section will be shown to be enhanced by an additional power of $\ln(W^2/m_q^2)$, i.e. the $\gamma\gamma$ total cross-section becomes a steeper function of W than the γp total cross-section, which seems to be confirmed experimentally. This enhancement will be a direct consequence of the singular behaviour of the photon wave function for small dipole sizes related to the point-like component of the photon. For simplicity, in the analysis given below, we focus on the contributions to the two-photon cross-sections of the light quarks u, d and s with the same mass $m_u = m_d = m_s = m_q$. The heavy flavour components exhibit the same general properties as the light flavour ones, but in the presently available kinematic range, the transition to the saturation regime may not be observed.

Let us first examine case (1) for the $\gamma\gamma$ total cross-section. The dominant contribution to the integrals in (8) comes from the region $4R_0^2(\bar{x}) \ll r_1^2 \ll r_2^2 \ll 1/m_q^2$, $4R_0^2(\bar{x}) \ll r_2^2 \ll r_1^2 \ll 1/m_q^2$, where $\bar{x} = 8m_q^2/W^2$ and $R_0(\bar{x})$ is given by (11). In this region the short distance approximation of the (transverse) photon wave function may be used

$$|\Psi_T(z, \mathbf{r})|^2 \sim \frac{1}{r^2}, \qquad (17)$$

and the corresponding contribution to the total $\gamma\gamma$ cross-section is

$$\sigma_{\gamma\gamma}(W^2) \sim \int_{4R_0^2(\bar{x})}^{1/m_q^2} \frac{{\rm d}r_2^2}{r_2^2} \int_{4R_0^2(\bar{x})}^{r_2^2} \frac{{\rm d}r_1^2}{r_1^2} \sim \ln^2[4R_0^2(\bar{x})m_q^2] \sim \ln^2(W^2/W_0^2). \qquad (18)$$

This should be compared with the γp total cross-section, where the saturation model extended down to the photoproduction limit gives $\sigma_{\gamma p}(W^2) \sim \ln(W^2/W_0^2)$.

Case (2) of the $\gamma^*\gamma^*$ cross-section in the configuration $Q_1^2 \sim Q_2^2 \sim Q^2$, with Q^2 being large, is regarded as a very useful tool for probing the bare "hard" pomeron exchange amplitude [35,36]. The short distance approximation (17) of the photon wave function is now valid in the region

$$r_k^2\, z_k(1 - z_k)\, Q_k^2 \ll 1, \quad k = 1, 2. \qquad (19)$$

The saturation model predicts different high energy behaviour of the $\gamma^*\gamma^*$ cross-section depending on whether $Q^2 > Q_{\rm s}^2(\bar{x})$ or $Q^2 < Q_{\rm s}^2(\bar{x})$, with the saturation scale $Q_{\rm s}^2(\bar{x}) \sim 1/R_0^2(\bar{x})$. Thus in the region $Q^2 > Q_{\rm s}^2(\bar{x})$ we get (modulo logarithmic corrections)

$$\sigma_{\gamma^*\gamma^*}(W^2, Q_1^2 \sim Q^2, Q_2^2 \sim Q^2) \sim \frac{1}{Q^2R_0^2(\bar{x})}, \qquad (20)$$

which exhibits the increase $W^{2\lambda}$ and $1/Q^2$ dependence, characteristic for the hard pomeron exchange. In the region $Q^2 < Q_{\rm s}^2(\bar{x})$ the $\gamma^*\gamma^*$ cross-section has the saturation property, i.e.

(a) the $1/Q^2$ behaviour is changed into a weakly varying function of Q^2;
(b) the power-like $W^{2\lambda}$ behaviour is replaced by a moderately increasing function of W^2.

The leading behaviour of $\sigma_{\gamma^*\gamma^*}$ for $Q^2R_0^2(\bar{x}) \ll 1$ comes from the "strongly ordered" configurations in the integrals (8) defining the $\gamma^*\gamma^*$ total cross-sections

$$\frac{1}{z_k(1-z_k)Q^2} \gg r_2^2 \gg r_1^2 \gg 4R_0^2(\bar{x}), \qquad (21)$$

with $k = 1$ and 2. From (8), (17) and (21) one obtains

$$\sigma_{\gamma^*\gamma^*}(W^2, Q_1^2 \sim Q^2, Q_2^2 \sim Q^2) \sim \ln^2(Q^2R_0^2(\bar{x}))[1 + \mathcal{O}(1/\ln(Q^2R_0^2(\bar{x})))]. \qquad (22)$$

Note that in the saturation model at high energies, the "pomeron" component of the $\gamma^*\gamma^*$ total cross-section is, to a good approximation, a function of only two variables, $\tau_1 = Q_1^2R_0^2(\bar{x})$ and $\tau_2 = Q_2^2R_0^2(\bar{x})$. An analogous "geometric scaling" was found in the DIS data [37]. A weak breaking of the scaling property in both cases occurs due to the presence of quark masses. For $Q_1^2 \sim Q_2^2 \sim Q^2$ (i.e. $\tau_1 \sim \tau_2 \sim \tau$), the $\gamma^*\gamma^*$ cross-section exhibits the $1/\tau$ behaviour at large τ (see (20)) and reaches the saturation limit corresponding to a slowly varying function of τ for small values of τ. It should be observed that the leading behaviour at small τ for the $\gamma^*\gamma^*$ total cross-section (see (22)) is more singular than for the γ^*p case, where $\sigma_{\gamma^*p} \sim \ln(1/\tau)$.

Finally, in case (3), corresponding to probing the structure of the real (or quasi-real) photons at low x and large Q^2, we find

$$F_2^\gamma(x, Q^2) \sim x^{-\lambda} \qquad (23)$$

for $Q^2 > Q_s^2(x)$ and

$$F_2^\gamma(x, Q^2) \sim Q^2 \ln^2[Q^2R_0^2(x)] \qquad (24)$$

for $Q_0^2 < Q^2 \ll Q_s^2(x)$.

2.4 Non-pomeron contributions

In order to get a complete description of the $\gamma^*\gamma^*$ interactions, which could be extended down to values of $W \sim 10$ GeV, we should add to the "pomeron" contribution defined by (8) the non-pomeron reggeon and QPM terms [36]. The additional contributions are characterised by a decreasing energy dependence, i.e. $\sim 1/W^{2\eta}$ for the reggeon and $\sim 1/W^2$ (with $\ln W$ corrections) for QPM. The QPM contribution, represented by the quark box diagrams, is well known and the cross-sections are given, for instance, in [38]. The reggeon contribution represents a non-perturbative phenomenon related to Regge trajectories of light mesons. It is known mainly from fits to total hadronic cross-sections and to the proton structure function F_2. A state-of-the-art parametrisation of the reggeon exchange cross-section in two-photon interactions is given by the following expression [24]

$$\sigma^R(W^2, Q_1^2, Q_2^2) = 4\pi^2\alpha_{\rm em}^2 \frac{A_2}{a_2}\left[\frac{a_2^2}{(a_2+Q_1^2)(a_2+Q_2^2)}\right]^{1-\eta}\left(\frac{W^2}{a_2}\right)^{-\eta}. \qquad (25)$$

Originally, the following values were set [24]: $A_2 = 0.38$, $a_2 = 0.3\,\mathrm{GeV}^2$ and $\eta = 0.45$. However, those parameters were obtained with certain assumptions concerning the pomeron exchange which are different from ours. Therefore, it is legitimate to modify the parameters of [24] while retaining its functional form. We have in particular found that in order to get a good description of the data on the $\gamma\gamma$ total cross-section in the "low" energy region, $W < 10\,\mathrm{GeV}$, one has to set $\eta = 0.3$. This happens to be consistent with the recent observation that the intercept of the f_2 trajectory, which contributes to the two-photon cross-section, can be expected to be equal to 0.7 [40]. We fitted the other parameters, A_2 and a_2, to the data on two-photon collisions.

Finally, note that the decomposition of the reggeon term into different photon polarisation states has not been specified. In our analysis we assume that the reggeon couples only to transverse photons. This arbitrary assumption does not influence significantly our results for the studied observables.

2.5 Threshold corrections

Strictly speaking, both the dipole model (accounting for the "pomerons") and the Regge model of the total cross-section are formulated in the high energy limit $x \simeq Q^2/W^2 \ll 1$. When extending the applicability of these models up to larger values of x, for instance $x \simeq 0.1$, threshold correction factors should be taken into account. Namely, the cross-section should vanish when $x \to 1$ as a power of $1 - x$. In the case of γ^*p scattering, the form of the cross-section at $x \simeq 1$ is governed by the number of spectator quarks $n_{\rm spect}$ in the proton which do not interact directly with the photon. To be precise, it follows from the dimensional-counting rules that for a subprocess with a given number of spectators, at $x \simeq 1$, the cross-section takes the form $\sigma_{\gamma^*p}(x, Q^2) \sim (1-x)^{2n_{\rm spect}-1}$ (where the Q^2 dependence is suppressed). A possible way to combine the small x dependence of the cross-section in the Regge model with the latter result is to include $(1-x)^{2n_{\rm spect}-1}$ as a multiplicative correction factor to the asymptotic cross-section from the pomeron or a subleading reggeon exchange [39]. For the pomeron exchange in γ^*p scattering one has $n_{\rm spect} = 4$ and for the other reggeons (f_2 and a_2), $n_{\rm spect} = 2$. It is clear that a similar procedure may be applied for the saturation model as well.

In the case of two-photon collisions, one of the photons plays the role of the target, probed by the other photon. In the dipole representation, the number of valence quarks in the target photon equals two, to be compared with three valence quarks in the proton.

Thus, for the non-pomeron reggeons one has $n_{\rm spect} = 1$ and for the dipole–dipole scattering component, which represents the "pomeron" exchange, one obtains $n_{\rm spect} = 3$. Recall that in order to extend the saturation model to describe real photons, we use the variable $\bar{x}_{ab}$ (see (10)) instead of x. Also, here we represent the threshold correction factors using $\bar{x}_{ab}$. Thus we multiply the reggeon term (25) by $(1-\bar{x}_{qq})$ with $\bar{x}_{qq}$ obtained from (10) with $m_a^2 = m_b^2 = m_q^2$, which is defined by the light quark mass m_q. For the dipole–dipole scattering cross-section, $\bar{x}_{ab}$ depends upon the flavour of quarks which span the dipoles. Hence, in our final formulae we multiply the dipole–dipole cross-section $\sigma^{dd}_{a,b}(\bar{x}_{ab}, r_1, r_2)$, (see (9)) by the factor $(1-\bar{x}_{ab})^5$.

2.6 Final formulae

For clarity, we collect the components of the two-photon cross-section presented above. The total $\gamma^*(Q_1^2)\gamma^*(Q_2^2)$ cross-section reads

$$\sigma^{\rm tot}_{ij}(W^2, Q_1^2, Q_2^2) = \tilde{\sigma}^G_{ij}(W^2, Q_1^2, Q_2^2) + \tilde{\sigma}^R(W^2, Q_1^2, Q_2^2)\delta_{i\rm T}\delta_{j\rm T} + \sigma^{\rm QPM}_{ij}(W^2, Q_1^2, Q_2^2), \quad (26)$$

where $\tilde{\sigma}^G_{ij}(W^2, Q_1^2, Q_2^2)$ is the gluonic component, corresponding to dipole–dipole scattering, as in (8), but with the dipole–dipole cross-section including the threshold correction factor

$$\tilde{\sigma}^{dd}_{a,b}(\bar{x}_{ab}, r_1, r_2) = (1-\bar{x}_{ab})^5 \sigma^{dd}_{a,b}(\bar{x}_{ab}, r_1, r_2), \quad (27)$$

cf. (9), and $\bar{x}_{ab}$ is given by (10). The subleading reggeon contributes only to scattering of two transversely polarised photons and also contains a threshold correction

$$\tilde{\sigma}^R(W^2, Q_1^2, Q_2^2) = (1-\bar{x})\sigma^R(W^2, Q_1^2, Q_2^2), \quad (28)$$

with

$$\bar{x} = \frac{Q_1^2 + Q_2^2 + 8m_q^2}{W^2 + Q_1^2 + Q_2^2}. \quad (29)$$

The third term $\sigma^{\rm QPM}_{i,j}(W^2, Q_1^2, Q_2^2)$ is the standard QPM contribution and is taken from [38].

3 Comparison to experimental data

3.1 Parameters of models

In the comparison to the data we study three models, based on all cases for the effective radius, as described in Sect. 2.2. We will refer to the these models as Model 1, 2 and 3, corresponding to the choice of the dipole–dipole cross-section. Let us recall that we take without any modification the parameters of the GBW model: $\sigma_0 = 29.13\,$mb, $x_0 = 0.41 \cdot 10^{-4}$ and $\lambda = 0.277$. However, we fit the light quark mass to the two-photon data, since it is not very well constrained by the GBW fit, as we explicitly verified. On the other hand, the sensitivity of the choice of the mass appears to be large for the two-photon total cross-section. We find that the optimal values of the light quark (u, d and s) masses m_q are 0.21, 0.23 and 0.30 GeV in Model 1, 2 and 3 respectively. Also, the masses of the charm and bottom quark are tuned within the range allowed by current measurements, to get the optimal global description in Model 1, $r^2_{\rm eff} = r_1^2 r_2^2/(r_1^2 + r_2^2)$, which agrees best with the data. For the charm quark we use $m_c = 1.3\,$GeV and for the bottom quark $m_b = 4.5\,$GeV. Moreover, we re-fit the η, A_2 and a_2 parameters in the reggeon term (25), which is legitimate because the "pomeron" term which we use is different from this following from the model of two pomerons used in [24]. We find that the values $\eta = 0.3$, $A_2 = 0.26$ and $a_2 = 0.2\,{\rm GeV}^2$ give the best description of data, when combined with the saturation model. The values of the masses listed above are consistently used also in the quark box contribution (QPM). The models which we shall mention from now on contain the saturation models described in Sect. 2, combined with the reggeon and QPM contribution.

It should be stressed that most of the data relevant for our study were collected with the help of the comprehensive review [41].

3.2 The test case: the γp total cross-section

As stated above, we modify the quark mass of the GBW saturation model and the Donnachie–Dosch–Rueter parametrisation for the subleading reggeon. Certainly, one has to ensure that this change does not spoil the quality of the GBW description. Besides that, it is necessary to check that the reggeon term with the modified exponent $\eta = 0.3$ allows the extension of the GBW model for the γp total cross-section down to low values of $W \sim 3\,$GeV as well. Thus we calculated the dipole–proton scattering contribution using the original GBW approach, with the light quark mass, m_q, set to 0.21 GeV, as in Model 1, and added the reggeon term

$$\sigma^R_{\gamma p}(W^2) = A_{\gamma p}\left(\frac{W^2}{1\,{\rm GeV}^2}\right)^{-\eta}, \quad (30)$$

where $A_{\gamma p}$ was fitted to the data and the best value reads $A_{\gamma p} = 0.135\,$mb. The result is given in Fig. 2, where the cross-section from Model 1 is compared to the data, taken from [43], and to the classical Donnachie–Landshoff fit [42]. In the same figure we also show the decomposition of the total cross-section into the gluonic contribution, given by the saturation model and the reggeon component. Both contributions have been multiplied by a correction factor of the form $(1-\bar{x})^{2n_{\rm spect}-1}$, as described in Sect. 2.5, with $n_{\rm spect} = 2$ for the reggeon exchange, and $n_{\rm spect} = 4$ for the dipole–proton scattering. The fitted curve, with only one free parameter, $A_{\gamma p}$, follows the data accurately, suggesting that the model has certain universal properties.

3.3 Total $\gamma\gamma$ cross-section

The available data for the $\gamma\gamma$ total cross-section range from the $\gamma\gamma$ energy W equal to about 1 GeV up to about

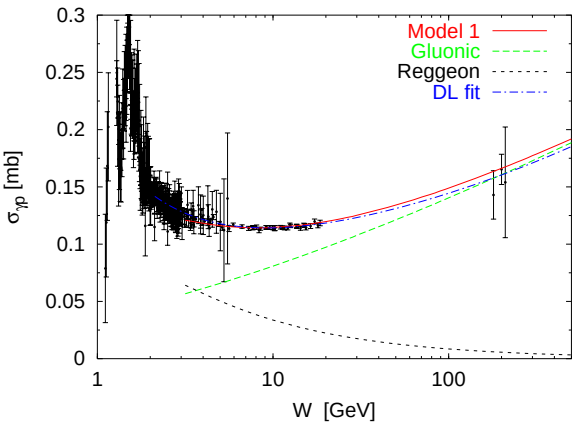

Fig. 2. The total γp cross-section; predictions from the GBW model with the light quark mass m_q set to 0.21 GeV and the charmed quark mass $m_c = 1.3\,\mathrm{GeV}$, supplemented by the reggeon term (30), compared to data and to the Donnachie–Landshoff fit [42]. Also shown are the gluonic and reggeon components of the full result in our model. The curves are cut at $W = 3\,\mathrm{GeV}$

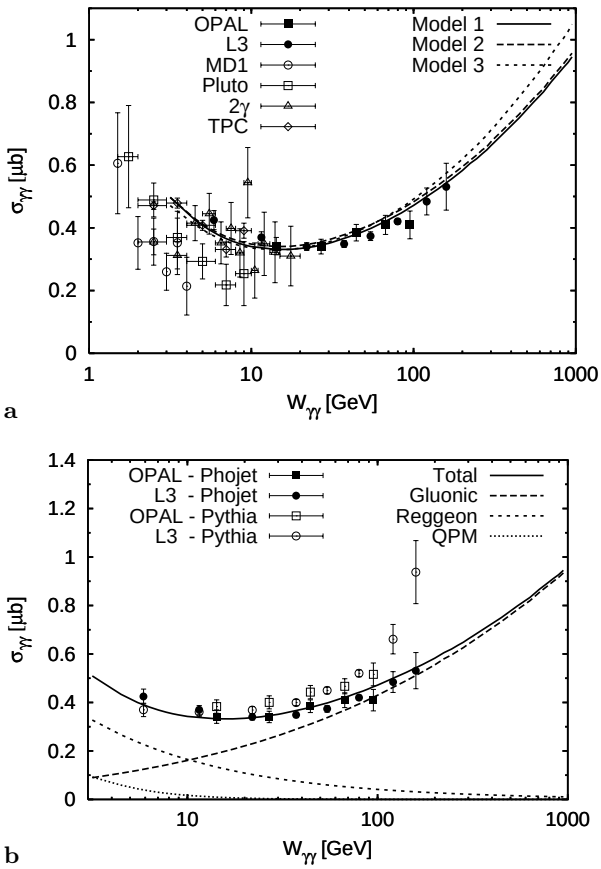

Fig. 3a,b. The total $\gamma\gamma$ cross-section: **a** data confronted with predictions from all three models and **b** contributions to the result of Model 1: gluonic, reggeon and QPM

160 GeV [44,45]; see Fig. 3. The experimental errors of the data are, unfortunately, rather large. One of the reasons is that those data were taken for virtual photons coming from electron beams and then the results were extrapolated to zero virtualities. Another problem appeared to be very important in LEP measurements where the incoming e^+ and e^- and a substantial fraction of the produced hadrons go into the beam pipe and cannot be detected. Extraction of the actual $\gamma\gamma$ collision energy is therefore needed from the visible energy, which is a model dependent procedure and introduces large systematic errors. In particular, it is well known that the data for the $\gamma\gamma$ total cross-section from LEP depend on the Monte Carlo method applied for the unfolding.

The data interpreted with Pythia [46] tend to be larger and exhibit a steeper increase with W than those unfolded with Phojet [47] (see Fig. 3b). In the saturation model it is difficult to obtain a cross-section consistent with the Pythia unfolded data. Besides that, Phojet is a Monte Carlo program dedicated to the description of two-photon interactions, and the description of the crucial hadron emissions close to the two-photon collision axis is elaborated in more detail. Thus we choose to follow the Phojet unfolded data in our analysis. In a more conservative approach one should include the difference between the cross-sections unfolded with different programs into the systematic error. This would only make the data less constraining and would not spoil the quality of the fit.

In Fig. 3a we show the total $\gamma\gamma$ cross-section from the models, obtained using (26) with $i = j = \mathrm{T}$. The agreement with the data is very good down to $W \simeq 3\,\mathrm{GeV}$. It is interesting to observe that the models strongly favour the Phojet unfolded data, and that the energy dependence of the total $\gamma\gamma$ cross-section (Phojet unfolded) at high W is very well reproduced by all three models; see Fig. 3b. Recall that the steeper W dependence found in the two-photon cross-section, as compared to the hadronic and the photoproduction cross-sections, is naturally explained by the presence of additional factors of $\ln^2 W$ and $\ln W$ respectively, as discussed in Sect. 2.3. Predictions for W in the range to be probed in future linear colliders (i.e. $W < 1\,\mathrm{TeV}$) are stable against variations of the details of the saturation models, provided that the models are adjusted to fit the available data.

3.4 Total $\gamma^*\gamma^*$ cross-section

The data [48,49] for the total $\gamma^*\gamma^*$ cross-section are extracted from so-called double tagged events; that is, from e^+e^- events in which both the scattered electrons are measured and hadrons are produced. In such events measurement of the kinematical variables of the leptons determines both the virtualities Q_1^2 and Q_2^2 of the colliding photons and the collision energy W. The tagging angles in LEP experiments restrict the virtualities to be similar, i.e. $Q_1^2 \sim Q_2^2 = Q^2$. The data are available from LEP for average values $Q^2 = 3.5\,\mathrm{GeV}^2$, $14\,\mathrm{GeV}^2$ and $Q^2 = 17.9\,\mathrm{GeV}^2$ in a wide range of W.

In Fig. 4a,b,c those data are compared with the curves from the models. As an estimate of the total $\gamma^*\gamma^*$ cross-section we use a simple sum of the cross-sections $\sigma_{ij}^{\mathrm{tot}}$ (see (26)) over transverse and longitudinal polarisations i and

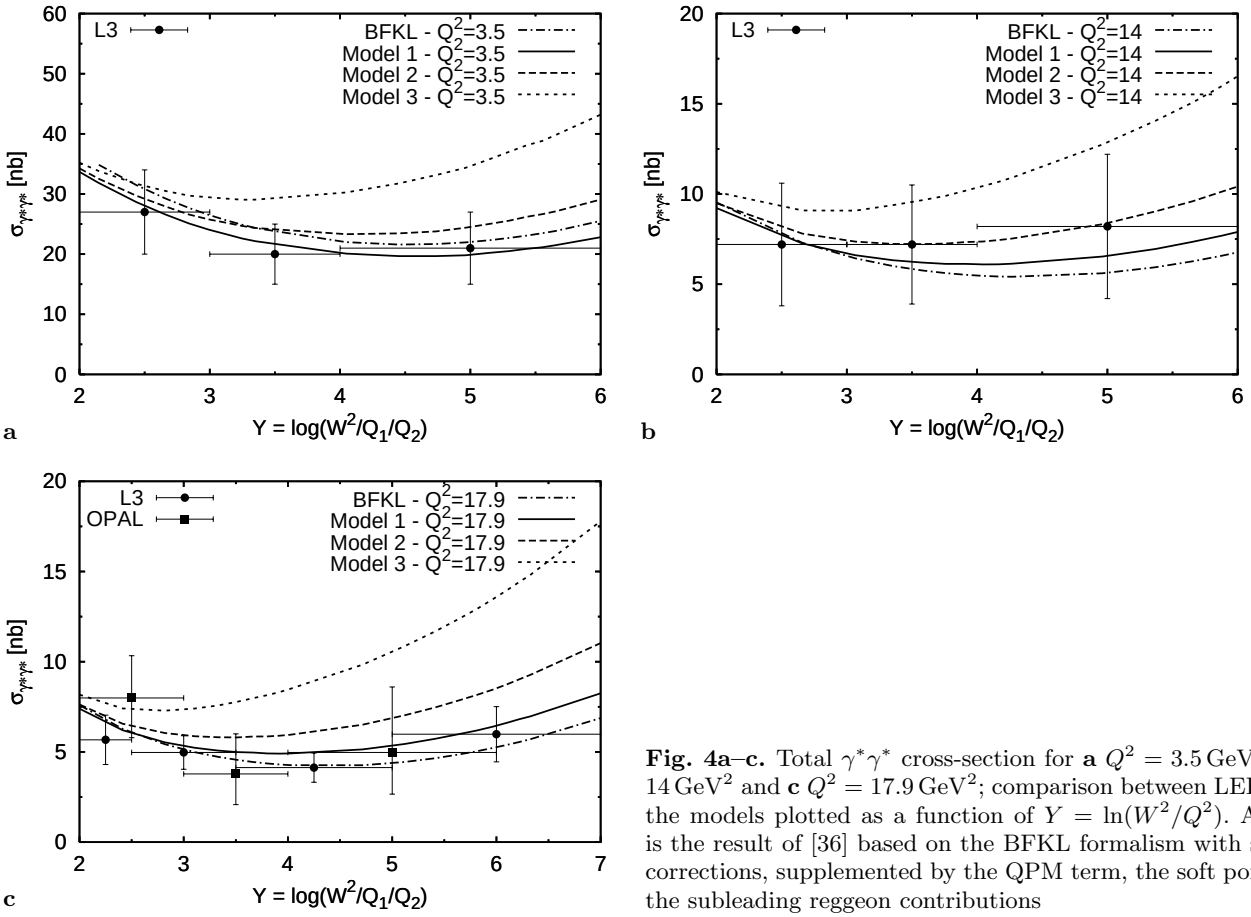

Fig. 4a–c. Total $\gamma^*\gamma^*$ cross-section for **a** $Q^2 = 3.5\,\mathrm{GeV}^2$, **b** $Q^2 = 14\,\mathrm{GeV}^2$ and **c** $Q^2 = 17.9\,\mathrm{GeV}^2$; comparison between LEP data and the models plotted as a function of $Y = \ln(W^2/Q^2)$. Also shown is the result of [36] based on the BFKL formalism with subleading corrections, supplemented by the QPM term, the soft pomeron and the subleading reggeon contributions

j of both photons. In addition we plot also the prediction obtained in [36] by solving the BFKL equation with non-leading effects, and we added phenomenological soft pomeron and reggeon contributions and the QPM term. The latter prediction was found to describe the measured e^+e^- differential cross-section for hadron production in double tagged events [36]. As can be seen, Model 1 fits the data as well as the result based on the BFKL solution. Model 2 is slightly worse than Model 1 and Model 3 may be rejected.

Since the virtuality Q^2 is high, the unitarity corrections are not important here. For the same reason, the results are not sensitive to the choice of the quark masses and the parameters of the reggeon term. As seen in Fig. 5, where the components of the $\gamma^*\gamma^*$ total cross-section from Model 1 are plotted, the cross-section is dominated by the QPM and the "pomeron" contributions. Moreover, the perturbative approximation for the photon wave function is fully justified in this case. Thus, in this measurement the form of the dipole–dipole cross-section is directly probed.

3.5 Photon structure

The quasi-real photon structure may be probed in single tagged e^+e^- events. In this case one of the electrons scatters with a larger momentum transfer $Q_1^2 = Q^2$ which corresponds to the emitted photon virtuality and the other electron scatters at a low angle, producing predominantly a virtual photon with very low virtuality, $Q_2^2 \simeq 0$. Thus, the measurement of the cross-section for the $\gamma^*(Q_1^2)\gamma^*(Q_2^2)$ collision at the energy W can be used to extract the almost real photon structure function $F_2^\gamma(x, Q^2)$, with $x = Q^2/(W^2 + Q^2)$; see (16).

Essentially, the parameters of the models are constrained by the data for the total $\gamma\gamma$ and $\gamma^*\gamma^*$ cross-sections so here we are presenting a parameter free result. In Fig. 6 we show the comparison of our predictions with the experimental data [50, 51] for the virtuality Q^2 in the range from (a) 1.9 to 2.8 GeV^2, (b) 3.7 to 5.1 GeV^2, (c) 8.9 to 12.0 GeV^2 and finally (d) from 16.0 to 23.1 GeV^2. Note that in each plot the data for various virtualities are combined, which may give rise to systematic effects; see for instance Fig. 6b. In each plot the value of the virtuality Q^2 adopted to obtain the theoretical curve is indicated and was selected to match the average value Q^2 of the data-set containing the best data at low x. We also show in Fig. 7 the contributions to F_2^γ in Model 1. As already stated, the importance of the reggeon term is not very large and decreases with increasing Q^2.

Model 1, favoured by the $\gamma^*\gamma^*$ data, provides the best description of F_2^γ as well. In the region of $x > 0.1$ the agreement of Model 1 with the data is surprisingly good, which was not a priori expected from the model based on the large energy approximation. Note however that a sys-

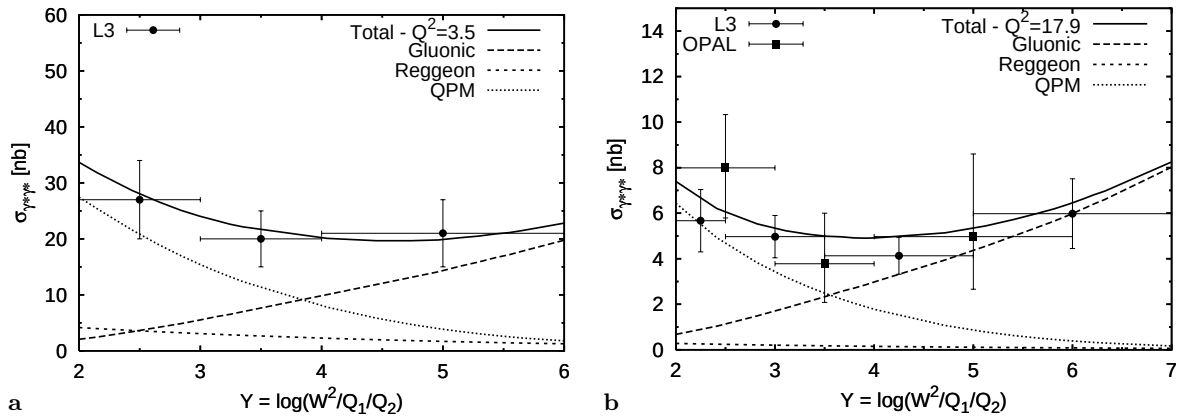

Fig. 5a,b. The total $\gamma^*\gamma^*$ cross-section; the decomposition of Model 1 into QPM, gluonic and reggeon components for **a** low virtuality, $Q^2 = 3.5\,\mathrm{GeV}^2$, and **b** large virtuality, $Q^2 = 17.9\,\mathrm{GeV}^2$

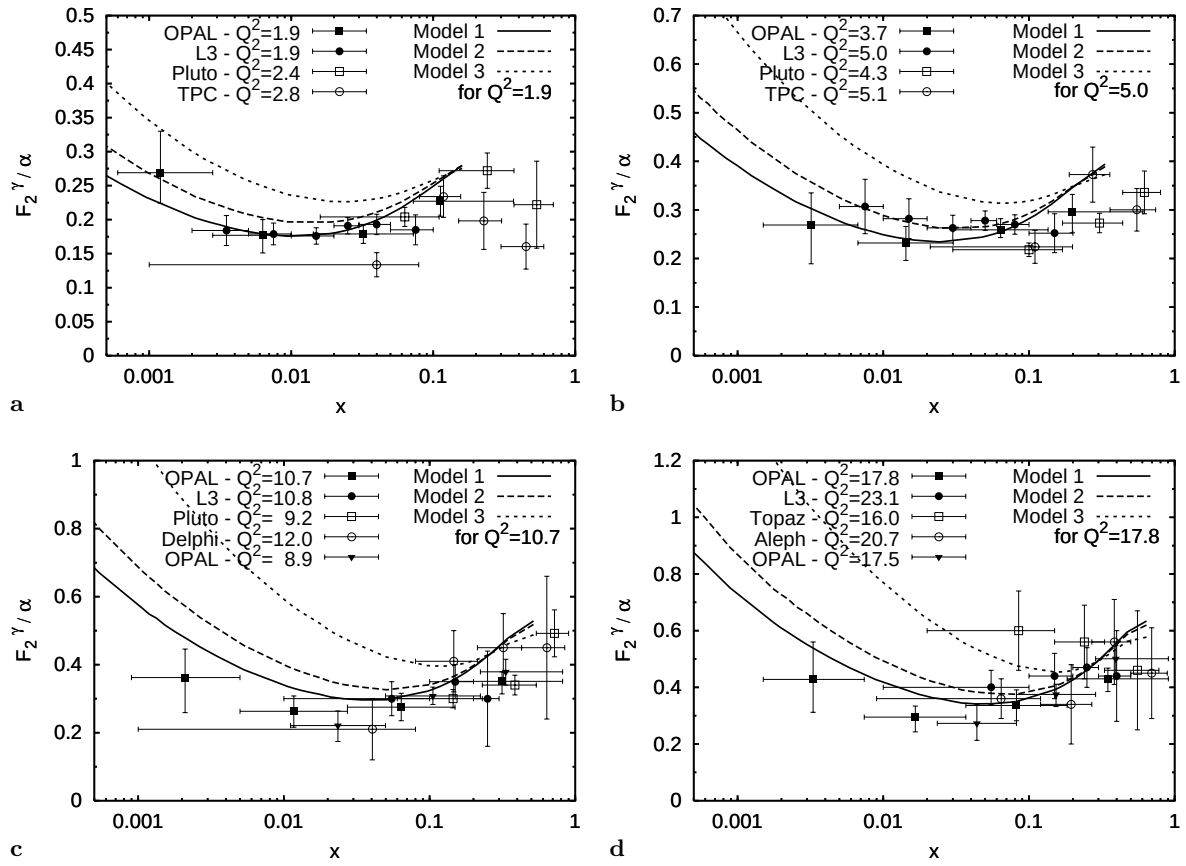

Fig. 6a–d. The photon structure function $F_2^\gamma(x, Q^2)$: the experimental data compared to predictions following from the models for various Q^2: **a** from 1.9 to $2.8\,\mathrm{GeV}^2$, **b** from 3.7 to $5.1\,\mathrm{GeV}^2$, **c** from 8.9 to $12.0\,\mathrm{GeV}^2$ and **d** from 16.0 to $23.1\,\mathrm{GeV}^2$. The curves are cut at values of x corresponding to $W = 3\,\mathrm{GeV}$

tematic tendency occurs for all the models to overestimate the data for larger Q^2.

It is straightforward to obtain in this framework predictions for the virtual photon (with $Q_2^2 = P^2$) structure function $F_2^{\gamma^*}(x, Q^2; P^2)$ in the low x domain. However, there exist only very few data on this observable so we do not present our predictions for this quantity. Nevertheless, possible experimental study of $F_2^{\gamma^*}(x, Q^2; P^2)$ would certainly provide another interesting test of the saturation model.

3.6 Heavy flavour production

Another interesting process which we have studied in the dipole model is the production of heavy flavours (charm

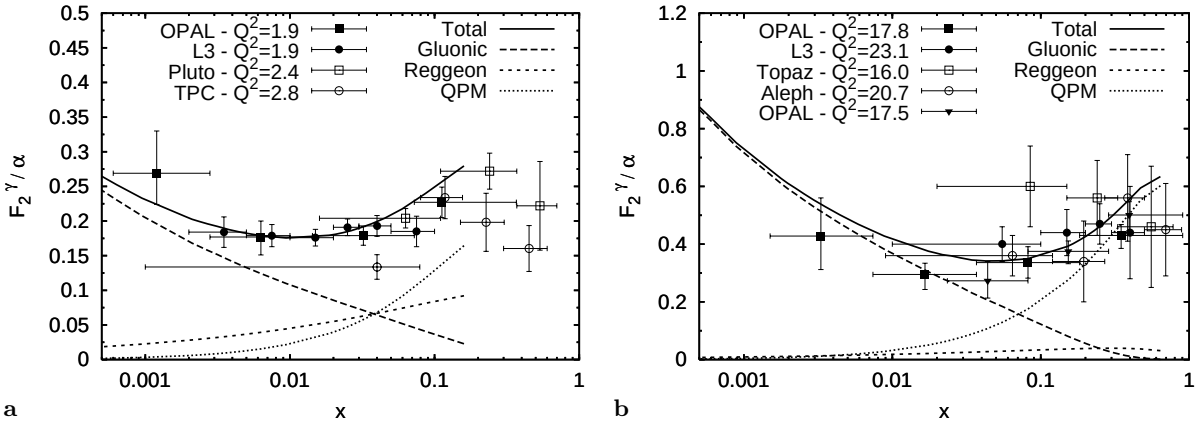

Fig. 7a,b. The photon structure function $F_2^\gamma(x, Q^2)$ from Model 1 compared to the experimental data for **a** low Q^2, 1.9 to 2.8 GeV^2, and **b** large Q^2, from 16.0 to 23.1 GeV^2

and bottom) in $\gamma\gamma$ collisions. Heavy quarks can be produced by three mechanisms:

(1) The direct production in which both photons couple to the same heavy quark line, which corresponds to a component of the quark box diagram (see Fig. 8a).
(2) The direct photoproduction off the resolved photon, which would involve a fluctuation of one of the photons into a heavy quark–antiquark pair and scattering of the pair off the other, resolved photon by exchange of gluons. This phenomenon is accounted for in the dipole model and the cross-section may be obtained by restricting the sum over the flavours in (2) to the case, in which at least one dipole is composed of the heavy quarks only (see Fig. 8b).
(3) The hard fragmentation and rescattering contributions. The first one corresponds to production of a heavy quark pair in the fragmentation process of an initial light quark pair. The initial pairs can be produced either through the box diagram (Fig. 8c) or as the colour dipoles (Fig. 8d) which are present in the model. Note also that in the saturation model, in the case of real photons and the original dipoles composed of light quarks, abundant rescattering of cascading gluons occurs in which heavy quarks may be produced. This would be the other, rescattering mechanism. The estimate of such effects is, so far, beyond the reach of our model and we do not take into account these contributions.

The reggeon exchange is a non-perturbative phenomenon and should not contribute to heavy flavour production, so it is assumed to vanish here. In Fig. 9 we plot the predictions from all three models compared with L3 data on charm production [52]. The best model, Model 1, is below the data, leaving some room for a possible contribution from the fragmentation. The shape of the cross-section is well reproduced.

Production of bottom quarks in two almost real photon collisions was investigated experimentally by the L3 [53] and the OPAL [54] collaborations. There, the measured process was $e^+e^- \to e^+e^-b\bar{b}X$, with anti-tagged

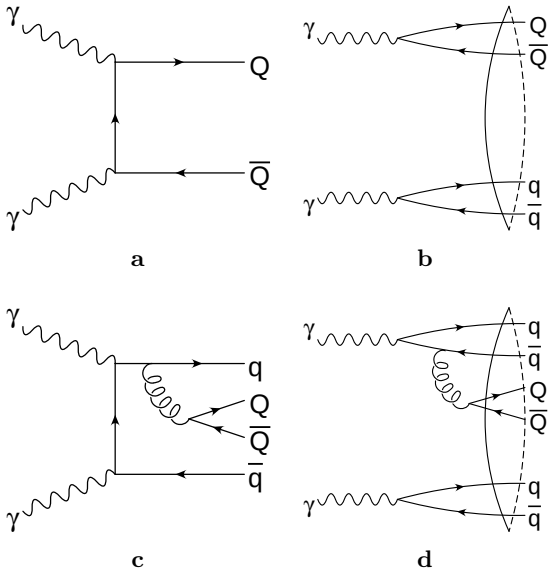

Fig. 8a–d. Diagrams illustrating contributions to the heavy quark production, at the amplitude level: **a** heavy quark box diagram, **b** direct production of heavy flavours in one of the dipoles, **c** example of production of a heavy quark pair through a hard fragmentation process in a box diagram, and **d** representation of production by hard fragmentation from a light quark dipole, or by gluon rescattering

electrons at e^+e^- invariant collision energies $s_{ee}^{1/2}$ between 189 GeV and 202 GeV. The total cross-section for this reaction was found to be $13.1 \pm 2.0\,(\text{stat}) \pm 2.4\,(\text{syst})$ pb (L3) and $14.2 \pm 2.5\,(\text{stat}) \pm 5\,(\text{syst})$ pb (OPAL), whereas the theoretical estimate from Model 1 for $s_{ee}^{1/2} = 200$ GeV gives about 5.5 pb with less than 10% uncertainty related to the choice of the b quark mass. This is significantly below the experimental data but above the expectations of 3 ± 1 pb (see e.g. [54]), based on standard QCD calculations with the use of the resolved photon approximation.

In conclusion, the saturation model underestimates the cross-section for production of heavy quarks and the discrepancy increases with increasing quark mass, or per-

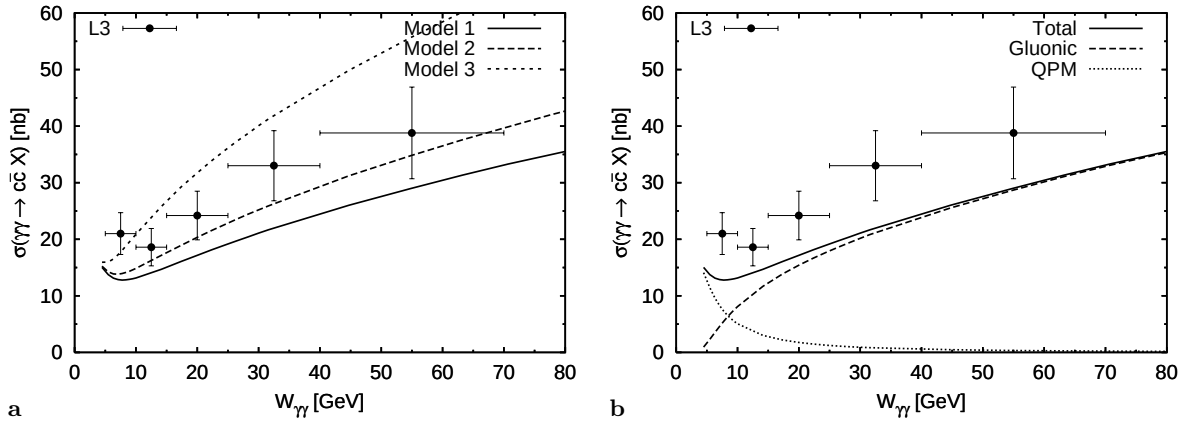

Fig. 9a,b. The cross-section for the inclusive charm production in $\gamma\gamma$ collisions: **a** results for all three models and **b** the decomposition of the result from Model 1 on the QPM and gluonic component

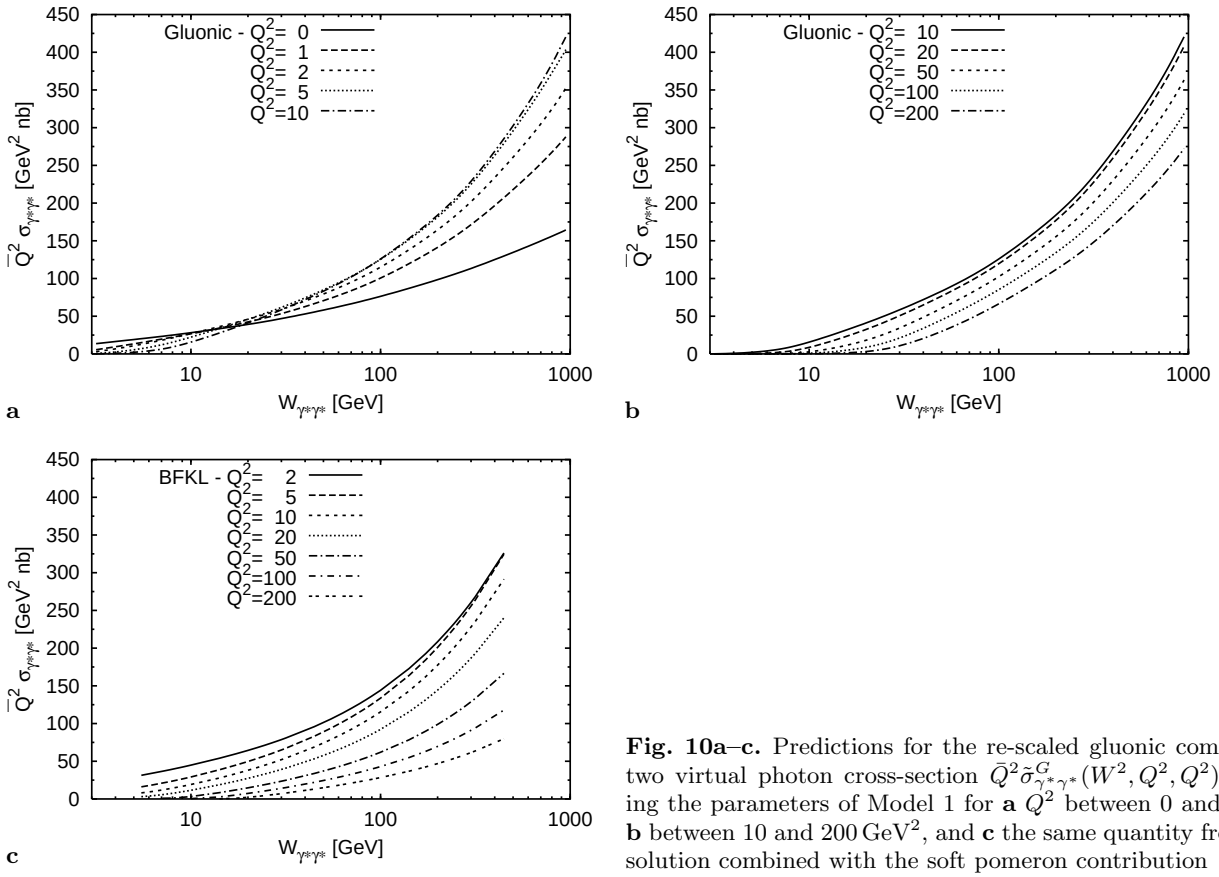

Fig. 10a–c. Predictions for the re-scaled gluonic component of the two virtual photon cross-section $\bar{Q}^2\tilde{\sigma}^G_{\gamma^*\gamma^*}(W^2, Q^2, Q^2)$ obtained using the parameters of Model 1 for **a** Q^2 between 0 and 10 GeV^2 and **b** between 10 and 200 GeV^2, and **c** the same quantity from the BFKL solution combined with the soft pomeron contribution

haps, decreasing electric charge. This may be a hint that the fragmentation and rescattering mechanisms of heavy quark production are, indeed, important.

4 Predictions for future colliders

Two-photon processes will be important at possible future e^+e^- colliders, like TESLA, where the available photon–photon collision energy might reach 500 GeV or even 1 TeV [55]. Thus, we give predictions from Model 1 for the energy dependence of $\gamma^*(Q^2)\gamma^*(Q^2)$, the *gluonic* component $\tilde{\sigma}^G_{\gamma^*\gamma^*}(W^2, Q^2, Q^2)$ (defined by (8) and (27)) of the total cross-section $\sigma^{\rm tot}_{\gamma^*\gamma^*}(Q_1^2, Q_2^2, W)$ for $Q_1^2 = Q_2^2 = Q^2$. In Fig. 10a,b we show the results in terms of a re-scaled quantity $\bar{Q}^2\tilde{\sigma}^G_{\gamma^*\gamma^*}(W^2, Q^2, Q^2)$, with $\bar{Q}^2 = \max(Q^2, 4m_q^2)$ for various Q^2 between 0 and 10 GeV^2 (Fig. 10a) and between 10 and 200 GeV^2 (Fig. 10b). Of course, the cross-section for gluon exchange $\tilde{\sigma}^G_{\gamma^*\gamma^*}(W^2, Q^2, Q^2)$ has to be combined with the standard QPM and reggeon terms in order to get a complete description of the total cross-section, as described in Sect. 2.6.

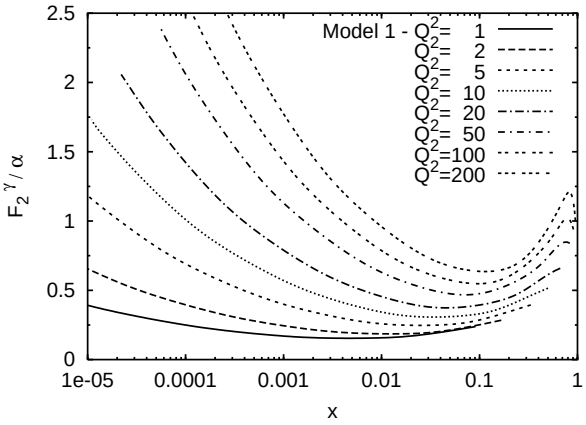

Fig. 11. The real photon structure function $F_2^\gamma(x, Q^2)$ for various Q^2 from Model 1

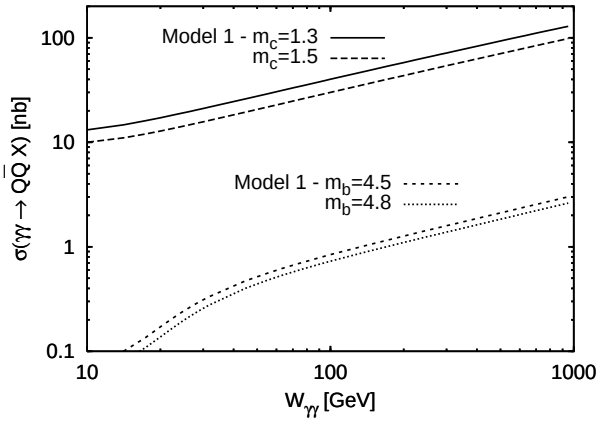

Fig. 12. Cross-sections for heavy quark production in two real photon collisions from Model 1

For comparison, the same quantity, but obtained from the solution of the BFKL equation with subleading corrections in the perturbative domain [36], is presented in Fig. 10c. Note that the latter result contains not only the perturbative BFKL part but also the soft pomeron contribution, obtained using the Regge factorisation. Recall that the relative importance of the soft pomeron term quickly decreases with increasing photon virtuality Q^2.

It is interesting to observe that in the saturation model, at higher W, where the threshold corrections are negligible, the quantity $\bar{Q}^2\tilde{\sigma}^G_{\gamma^*\gamma^*}(W^2, Q^2, Q^2)$ increases with Q^2 up to about $10\,\mathrm{GeV}^2$; see Fig. 10a, and for $Q^2 > 10\,\mathrm{GeV}^2$ it decreases with Q^2. The reason for the increase for smaller Q^2 is the increasing contribution from the charmed quark dipoles. The relative suppression of the charmed quark contribution at $Q^2 = 0$, in comparison to the light quarks due to the higher charm mass, is becoming less important towards higher $Q^2 > 4m_c^2$, when the typical scales in those two cases become similar.

On the other hand, the bottom quark has a relatively small charge of $1/3\,e$ and such threshold effects are much less pronounced. Thus, for $Q^2 > 4m_c^2$ the cross-section should enter the geometric scaling regime. The unitarity corrections may be neglected at higher Q^2 and it follows that $\bar{Q}^2\tilde{\sigma}^G_{\gamma^*\gamma^*}(W^2, Q^2, Q^2) \sim (W^2/Q^2)^\lambda$, modulo threshold corrections. This is the reason why one sees a monotonical decrease of $\bar{Q}^2\tilde{\sigma}^G_{\gamma^*\gamma^*}(W^2, Q^2, Q^2)$ with Q^2 in Fig. 10b.

For Q^2 in the perturbative domain, the difference between the results from the saturation model and the BFKL predictions is not large but grows with Q^2. The tendency of $\bar{Q}^2\tilde{\sigma}^G_{\gamma^*\gamma^*}(W^2, Q^2, Q^2)$ to decrease with increasing Q^2 in the BFKL approach may be traced back to important threshold effects and the running of the QCD coupling, which were taken into account in [36].

Let us also recall that the prediction for the $\gamma\gamma$ total cross-section for W in the TeV range is not sensitive to the choice of the form of the dipole–dipole cross-section; see Fig. 3. However, it does rely on the accuracy of the data unfolding with Phojet. Thus, the systematic uncertainty of the data unfolding at LEP propagates into the model predictions.

In Fig. 11 the real photon structure $F_2^\gamma(x, Q^2)$ is plotted for various Q^2 between $1\,\mathrm{GeV}^2$ and $200\,\mathrm{GeV}^2$ for x down to 10^{-5}. The kinematical range was chosen to be relevant for the future linear collider measurements. For completeness, in Fig. 12 we also give the dependence of the cross-section for heavy quarks production in $\gamma\gamma$ collisions in a wide range of two-photon collision energy W. We indicate the effect of the quark mass variation both for charm and for bottom. One should, however, keep in mind that the saturation model in the present form gives slightly too low cross-sections for c quarks production and significantly too low (by a factor of about 2–2.5) for b quarks.

5 Conclusions

In this paper we have extended the saturation model proposed by Golec-Biernat and Wüsthoff for $\gamma^* p$ cross-sections, to describe two-photon processes at high energies. This extension required an explicit model for the scattering of two colour dipoles. We considered three models of this cross-section, all of them exhibiting the essential feature of colour transparency for small dipoles, and the saturation property for large ones. We kept the GBW form of the unitarising function and the original parameters, except for changing the values of quark masses, which was necessary to describe the data on the total two real photon cross-section.

We have explicitly checked that these modifications had not spoiled the fit to photoproduction data. In order to obtain a more complete description applicable at lower energies the saturation model has been combined with other, well-known contributions related to the quark box diagram and non-pomeron reggeon exchange. Those mechanisms become dominant when the collision energy is comparable to photon virtualities and quark masses. Standard multiplicative threshold correction factors, relevant for lower energies, have been included into the saturation model and the subleading reggeon contribution.

We have analysed general features of the saturation model for the $\gamma\gamma$ scattering. We observed that such mod-

els gave an energy (W) dependence for two-photon total cross-section in the saturation regime steeper than the photon–hadron and hadron–hadron total cross-sections, by additional factors of $\ln W$ and $\ln^2 W$ respectively. In the non-saturated regime, a typical power-like growth $W^{2\lambda}$, $\lambda \simeq 0.3$, with energy was obtained, characteristic for the hard pomeron exchange.

The results from the studied models were compared with the data for different two-photon processes at high rapidity values: the total $\gamma\gamma$ cross-section, the total $\gamma^*\gamma^*$ cross-section for similar virtualities of the photons, the real photon structure function F_2^γ and heavy flavour production. Free parameters of the models were fitted to the data. It was found that the data favour one of the models for the dipole–dipole cross-section, namely Model 1 presented in Sects. 2.2 and 3.1. With this model a reasonable global description of the available two-photon data was obtained, except for the b quark production. Predictions for energies accessible at future linear colliders were formulated. It is however encouraging that Model 2 (see Sects. 2.2 and 3.1), being a significantly different generalisation of the original GBW model, gives results close to Model 1, with a relative difference of less than 15%. This means that the sensitivity of the predictions of the saturation model to the details is not very significant.

In summary, the saturation model was found to provide a simple and efficient framework to calculate observables in two-photon processes. This success supports strongly the idea of a rapidity dependent saturation scale and improves the understanding of two-photon physics.

Acknowledgements. We are indebted to Rikard Enberg for his contribution at the early stage of this work and his useful remarks. We thank Barbara Badełek and Gunnar Ingelman for reading the manuscript and their comments. LM is grateful to the Swedish Natural Science Research Council for the fellowship. This research was partially supported by the EU Fourth Framework Programme "Training and Mobility of Researchers", Network "Quantum Chromodynamics and the Deep Structure of Elementary Particles", contract FMRX–CT98–0194 and by the Polish Committee for Scientific Research (KBN) grants no. 2P03B 05119 and 5P03B 14420.

References

1. L.V. Gribov, E.M. Levin, M.G. Ryskin, Phys. Rep. **100**, 1 (1983)
2. A.H. Mueller, J. Qiu, Nucl. Phys. B **268**, 427 (1986)
3. N.N. Nikolaev, B.G. Zakharov, Z. Phys. C **49**, 607 (1991); Z. Phys. C **53**, 331 (1992); Z. Phys. C **64**, 651 (1994); JETP **78**, 598 (1994)
4. A.H. Mueller, Nucl. Phys. B **415**, 373 (1994); A.H. Mueller, B. Patel, Nucl. Phys. B **425**, 471 (1994); A.H. Mueller, Nucl. Phys. B **437**, 107 (1995)
5. A.H. Mueller, Nucl. Phys. B **335**, 115 (1990); Yu.A. Kovchegov, A.H. Mueller, S. Wallon, Nucl. Phys. B **507**, 367 (1997); A.H. Mueller, Eur. Phys. J. A **1**, 19 (1998); Nucl. Phys. A **654**, 370 (1999); Nucl. Phys. B **558**, 285 (1999)
6. J.C. Collins, J. Kwieciński, Nucl. Phys. B **335**, 89 (1990); J. Bartels, G.A. Schuler, J. Blümlein, Z. Phys. C **50**, 91 (1991); Nucl. Phys. Proc. Suppl. **18**, C 147 (1991)
7. J. Bartels, E.M. Levin, Nucl. Phys. B **387**, 617 (1992); J. Bartels, Phys. Lett. B **298**, 204 (1993); Z. Phys. C **60**, 471 (1993); Z. Phys. C **62**, 425 (1994); J. Bartels, M. Wüsthoff, Z. Phys. C **66**, 157 (1995); J. Bartels, C. Ewerz, JHEP **9909**, 026 (1999)
8. L. McLerran, R. Venugopalan, Phys. Rev. D **49**, 2233 (1994); Phys. Rev. D **49**, 3352 (1994); Phys. Rev. D **50**, 2225 (1994); A. Kovner, L. McLerran, H. Weigert, Phys. Rev. D **52**, 6231 (1995); Phys. Rev. D **52**, 3809 (1995); R. Venugopalan, Acta Phys. Polon. B **30**, 3731 (1999); E. Iancu, L. McLerran, Phys. Lett. B **510**, 145 (2001); L. McLerran, hep-ph/0104285; E. Iancu, A. Leonidov, L. McLerran, Nucl. Phys. A **692**, 583 (2001); E. Ferreiro, E. Iancu, A. Leonidov, L. McLerran, hep-ph/0109115; A. Capella et al., Phys. Rev. D **63**, 054010 (2001)
9. G.P. Salam, Nucl. Phys. B **449**, 589 (1995); Nucl. Phys. B **461**, 512 (1996); Comput. Phys. Commun. **105**, 62 (1997); A.H. Mueller, G.P. Salam, Nucl. Phys. B **475**, 293 (1996)
10. E. Gotsman, E.M. Levin, U. Maor, Nucl. Phys. B **464**, 251 (1996); Nucl. Phys. B **493**, 354 (1997); Phys. Lett. B **245**, 369 (1998); Eur. Phys. J. C **5**, 303 (1998); E. Gotsman, E.M. Levin, U. Maor, E. Naftali, Nucl. Phys. B **539**, 535 (1999); A.L. Ayala Filho, M.B. Gay Ducati, E.M. Levin, Nucl. Phys. B **493**, 305 (1997); Nucl. Phys. B **551**, 355 (1998); Eur. Phys. J. C **8**, 115 (1999)
11. Ia. Balitsky, Nucl. Phys. B **463**, 99 (1996)
12. J. Jalilian-Marian, A. Kovner, L. McLerran, H. Weigert, Phys. Rev. D **55**, 5414 (1997); J. Jalilian-Marian, A. Kovner, H. Weigert, Phys. Rev. D **59**, 014014 (1999); Phys. Rev. D **59**, 014015 (1999); Phys. Rev. D **59**, 034007 (1999); Erratum ibid. D **59**, 099903 (1999); A. Kovner, J. Guilherme Milhano, H. Weigert, Phys. Rev. D **62**, 114005 (2000); H. Weigert, NORDITA-2000-34-HE, hep-ph/0004044
13. M.A. Braun, Eur. Phys. J. C **16**, 337 (2000); hep-ph/0101070
14. Yu.V. Kovchegov, L. McLerran, Phys. Rev. D **60**, 054025 (1999); Erratum ibid. D **62**, 019901 (2000); Yu.V. Kovchegov, E.M. Levin, Nucl. Phys. B **577**, 221 (2000); Yu.V. Kovchegov, Phys. Rev. D **60**, 034008 (1999); Phys. Rev. D **61**, 074018 (2000)
15. E.M. Levin, K. Tuchin, Nucl. Phys. B **537**, 833 (2000); Nucl. Phys. A **691**, 779 (2001); ibid. A **693**, 787 (2001)
16. K. Golec-Biernat, M. Wüsthoff, Phys. Rev. D **59**, 014017 (1998)
17. E.A. Kuraev, L.N. Lipatov, V.S. Fadin, Sov. Phys. JETP **44**, 443 (1976); ibid. **45**, 199 (1977); I.I. Balitsky, L.N. Lipatov, Sov. J. Nucl. Phys. **28**, 822 (1978)
18. A.M. Cooper-Sarkar, R.C.E. Devenish, A. De Roeck, Int. J. Mod. Phys. C **7**, 609 (1999)
19. K. Golec-Biernat, M. Wüsthoff, Phys. Rev. D **60**, 114023 (1999)
20. E. Gotsman, A. Levy, U. Maor, Z. Phys. C **40**, 117 (1988)
21. G.A. Schuler, Comput. Phys. Commun. **108**, 279 (1998)
22. G.A. Schuler, T. Sjöstrand, Z. Phys. C **73**, 677 (1997)
23. A. Donnachie, H.G. Dosch, M. Rueter, Phys. Rev. D **59**, 074011 (1999); H.G. Dosch, Nucl. Phys. Proc. Suppl. **96**, 118 (2001)
24. A. Donnachie, H.G. Dosch, M. Rueter, Eur. Phys. J. C **13**, 141 (2000)

25. N.N. Nikolaev, J. Speth, V.R. Zoller, hep-ph/0001120
26. E. Gotsman et al., Eur. Phys. J. C **14**, 511 (2000)
27. B. Badełek, J. Kwieciński, A.M. Staśto, Acta Phys. Polon. B **30**, 1807 (1999)
28. B. Badełek, M. Krawczyk, J. Kwieciński, A.M. Staśto, Phys. Rev. D **62**, 074021 (2000)
29. J.R. Forshaw, J.K. Storrow, Phys. Rev. D **46**, 4955 (1992); Phys. Lett. B **278**, 193 (1992)
30. A. Corsetti, R.M. Godbole, G. Pancheri, Phys. Lett. B **435**, 441 (1998) and references therein; R.M. Godbole, A. Grau, G. Pancheri, Nucl. Phys. Proc. Suppl. **82**, 246 (2000); R.M. Goodbole, G. Pancheri, Nucl. Instrum. Meth. A **472**, 205 (2001)
31. B. Badełek, J. Kwieciński, Rev. Mod. Phys. **68**, 445 (1996)
32. S. Catani, M. Ciafaloni, F. Hautmann, Phys. Lett. B **242**, 97 (1990); Nucl. Phys. B **366**, 135 (1991); J.C. Collins, R.K. Ellis, Nucl. Phys. B **360**, 3 (1991); S. Catani, F. Hautmann, Nucl. Phys. B **427**, 475 (1991)
33. A. Białas, H. Navelet, R. Peschanski, Nucl. Phys. B **593**, 438 (2001)
34. A. Donnachie, P.V. Landshoff, Phys. Lett. B **437**, 408 (1998)
35. S.J. Brodsky, F. Hautmann, D.A. Soper, Phys. Rev. D **56**, 6957 (1997); Phys. Rev. Lett. **78**, 803 (1997); Erratum ibid. **79**, 3544 (1997); J. Bartels, A. De Roeck, H. Lotter, Phys. Lett. B **389**, 742 (1996); J. Bartels, A. De Roeck, C. Ewerz, H. Lotter, hep-ph/9710500; W. Florkowski, Acta Phys. Polon. B **28**, 2673 (1997); A. Białas, W. Czyż, W. Florkowski, Eur. Phys. J. C **2**, 683 (1998); M. Boonekamp et al., Nucl. Phys. B **555**, 540 (1999); V.T. Kim, L. Lipatov, G.B. Pivovarov, hep-ph/9911228; J. Bartels, C. Ewerz, R. Staritzbichler, Phys. Lett. B **492**, 56 (2000)
36. J. Kwieciński, L. Motyka, Acta Phys. Polon. B **30**, 1817 (1999); Phys. Lett. B **462**, 203 (1999); Eur. Phys. J. C **18**, 343 (2000)
37. A. Staśto, K. Golec-Biernat, J. Kwieciński, Phys. Rev. Lett. **86**, 56 (2001)
38. V.M. Budnev, I.F. Ginzburg, C.V. Meledin, V.G. Serbo, Phys. Rep. **15**, 181 (1974)
39. A. Donnachie, P.V. Landshoff, Phys. Lett. B **518**, 63 (2001)
40. P.V. Landshoff, hep-ph/0010315
41. M. Krawczyk, A. Zembrzuski, M. Staszel, Phys. Rep. **345**, 265 (2001)
42. A. Donnachie, P.V. Landshoff, Phys. Lett. B **296**, 227 (1992); Z. Phys. C **61**, 139 (1994)
43. D.E. Groom et al. [Particle Data Group Collaboration], Eur. Phys. J. C **15**, 1 (2000)
44. C. Berger et al. [PLUTO Collaboration], Z. Phys. C **26**, 353 (1984); C. Berger et al. [PLUTO Collaboration], Phys. Lett. B **149**, 421 (1984); D. Bintinger et al. [TPC/Two Gamma Collaboration], Phys. Rev. Lett. **54**, 763 (1985); H. Aihara et al. [TPC/Two Gamma Collaboration], Phys. Rev. D **41**, 2667 (1990); S.E. Baru et al., Z. Phys. C **53**, 219 (1992)
45. G. Abbiendi et al. [OPAL Collaboration], Eur. Phys. J. C **14**, 199 (2000); M. Acciarri et al. [L3 Collaboration], Phys. Lett. B **519**, 33 (2001)
46. T. Sjöstrand, P. Eden, C. Friberg, L. Lönnblad, G. Miu, S. Mrenna, E. Norrbin, Comput. Phys. Commun. **135**, 238 (2001)
47. R. Engel, J. Ranft, Phys. Rev. D **54**, 4244 (1996)
48. M. Acciarri et al. [L3 Collaboration], Phys. Lett. B **453**, 333 (1999); L3 Note 2680, contribution to EPS-HEP conference in Budapest, July 2001
49. G. Abbiendi et al. [OPAL Collaboration], hep-ex/0110006
50. C. Berger et al. [PLUTO Collaboration], Phys. Lett. B **142**, 111 (1984); H. Aihara et al. [TPC/Two Gamma Collaboration], Z. Phys. C **34**, 1 (1987); C. Berger et al. [PLUTO Collaboration], Nucl. Phys. B **281**, 365 (1987); K. Muramatsu et al. [TOPAZ Collaboration], Phys. Lett. B **332**, 477 (1994)
51. M. Acciarri et al. [L3 Collaboration], Phys. Lett. B **436**, 403 (1998); M. Acciarri et al. [L3 Collaboration], Phys. Lett. B **447**, (1999) 147; G. Abbiendi et al. [OPAL Collaboration], Eur. Phys. J. C **18**, 15 (2000); R. Barate et al. [ALEPH Collaboration], Phys. Lett. B **458**, 152 (1999); P. Abreu et al. [DELPHI Collaboration], Z. Phys. C **69**, 223 (1996)
52. M. Acciarri et al. [L3 Collaboration], Phys. Lett. B **514**, 19 (2001)
53. M. Acciarri et al. [L3 Collaboration], Phys. Lett. B **503**, 10 (2001)
54. The OPAL Collaboration, OPAL Physics Note PN455
55. J.A. Aguilar-Saavedra et al. [ECFA/DESY LC Physics Working Group Collaboration], hep-ph/0106315; B. Badełek et al. [TESLA-N Study Group Collaboration], Nucl. Instr. Meth. A **472**, 1 (2001) [hep-ex/0108012]